Physica B 685 (2024) 415970

Contents lists available at ScienceDirect

Physica B: Condensed Matter

journal homepage: www.elsevier.com/locate/physb

Plasmon-exciton interactions in ZnO/AuNPs heterostructure film for high photoconductivity

Qais M. Al-Bataineh [a,b,*], Ahmad A. Ahmad [c,**], A.B. Migdadi [c], A. Bahti [a,b], Ahmad Telfah [d,e]

[a] Leibniz Institut für Analytische Wissenschaften-ISAS-e.V., Bunsen-Kirchhoff-Straße 11, 44139, Dortmund, Germany
[b] Experimental Physics, TU Dortmund University, 44227, Dortmund, Germany
[c] Department of Physics, Jordan University of Science and Technology, P.O. Box 3030, Irbid, 22110, Jordan
[d] Cell Therapy Center, The University of Jordan, 11942, Amman, Jordan
[e] Fachhochschule Dortmund University of Applied Sciences and Arts, 44139, Dortmund, Germany

ARTICLE INFO

Keywords:
Plasmon-exciton interactions
Zinc oxide (ZnO)
Gold nanoparticles (AuNPs)
Heterostructure film
Absorption coefficient
Photoconductivity

ABSTRACT

This study investigatesplasmon-exciton interactions within ZnO/AuNPs heterostructure films. Elemental, structural, and morphological analyses validate the successful formation of these films. The observed shift in the plasmonic resonance band and absorption edge otowards the red region the red region is attributed to strong surface plasmon damping influenced by exciton interactions within ZnO. Irradiation with blue light induces plasmonic electrons, generation in the ZnO/AuNPs film, enhancing electrical conductivity through interaction with ZnO excitonic states. UV light irradiating generates the electron-hole pair in the ZnO film and interacts with the free electrons in AuNPs. The ZnO/AuNPs heterostructure films hold promise for applications such as high-performance UV-photodetectors, photoactive layers in solar cells, light-emitting diodes, and energy storage devices.

1. Introduction

The interactions between light and nanostructures are essential in optical and optoelectronic applications, including sensors, quantum computing, and optoelectronic nanodevices [1–3]. Plasmonic and high refractive index nanostructures are the primary examples of controlling light-matter interactions [4–6]. The photoelectronic, photovoltaic, and photocatalyst materials-based semiconductors, including zinc oxide, titanium dioxide, cerium dioxide, and others have been widely investigated for various applications, including optoelectronic devices, solar cells, solar water splitting, and water treatment [7]. However, these semiconductors have wide bandgap energy (>3.0 eV) and primarily absorb UV light (~4 % of solar radiation) [7,8]. Consequently, there has been significant interest among researchers in developing novel materials and strategies to convert visible light (~42 % of solar radiation) into usable energy.

Recently, heterostructure films have attracted global attention due to their unique phase morphologies, offering new avenues to investigate different novel phenomena [9]. Among metal oxides, zinc oxide (ZnO) holds significant promise for a wide range of applications, including optoelectronics [10,11], photodetectors [12], LED [13], solar cells [14–16], sensors [17], and other optical coating applications [18]. This can be attributed to its distinguishing characteristics, including wide direct bandgap energy (3.37 eV), high transparency in the visible region (≥80 %), and high semiconductor resistivity (1–100 Ω cm) [19–23]. Additionally, ZnO is an n-type semiconductor due to the existence of H impurities associated with the oxygen vacancies (V_0), which act as shallow donors [24]. ZnO also exhibits a large exciton binding energy (approximately 60 meV), ensuring more efficient excitonic emission, particularly at higher temperatures [20].

In addition to excitons, plasmonic nanostructures exhibit light-matter interactions due to localized surface plasmon resonances (LSPRs). Surface plasmons are arise from the strong interaction between the EM photons and the electrons on the metal surface, which have a huge potential for future photonic device applications [25,26]. Among various metal nanoparticles, gold nanoparticles (AuNPs) are widely used in optoelectronics, sensors, catalysis, and nanomedicine, due to their surface plasmon resonance (SPR), as well as their chemical and physical stability, biocompatibility, and easy surface functionalization [27].

Excitons and plasmons represent two common excited states known

* Corresponding author. Leibniz Institut für Analytische Wissenschaften-ISAS-e.V., Bunsen-Kirchhoff-Straße 11, 44139, Dortmund, Germany.
** Corresponding author. Department of Physics, Jordan University of Science and Technology, P.O. Box 3030, Irbid, 22110, Jordan.
E-mail address: qais.albataineh@tu-dortmund.de (Q.M. Al-Bataineh).

https://doi.org/10.1016/j.physb.2024.415970
Received 7 August 2023; Accepted 13 April 2024
Available online 14 April 2024
0921-4526/© 2024 The Authors. Published by Elsevier B.V. This is an open access article under the CC BY license (http://creativecommons.org/licenses/by/4.0/).

for for producing coupled electronic systems [28]. Therefore, incorporating plasmonic nanoparticles into semiconductors holds great promise for enhancing solar energy conversion efficiency. In this study, the plasmon-exciton interactions between ZnO and Au in ZnO/AuNPs heterostructure film were investigated. The ZnO/AuNPs heterostructure film was fabricated by depositing AuNPs onto the ZnO film that was coated on the ITO substrate. The elemental, structural, and morphological properties were characterized to ensure the success of building ZnO/AuNPs heterostructure film. Subsequently, optical absorption coefficient spectra and 2D electrical conductivity maps were analyzed to investigate the plasmon-exciton interactions between Au and ZnO within ZnO/AuNPs heterostructure film. The potential use of ZnO/AuNPs heterostructure film as a photodetector was explored by studying its photoconductivity.

2. Experimental procedure

2.1. Film deposition

All chemicals were obtained from Sigma-Aldrich without any modifications. Following our previous research [29], a ZnO stock solution was prepared by mixing zinc acetate dehydrate (183.48 g/mol, 4.38 g), ethanolamine (≥99.0 %, 1.7 mL), and absolute ethanol (≥99.5 %, 50 mL) using a magnetic stirrer for 2 h at room temperature until a transparent homogeneous solution was obtained. ZnO stock solution was then filtered using 0.45 μm filter paper before use. ITO glass substrates (250 nm ITO on glass) were cleaned by sonicating in acetone and isopropyl alcohol for 30 min at ambient conditions. ZnO film was deposited on the ITO substrate by immersing the ITO substrate in the final ZnO stock solution for 2 h to achieve thickness of 500 nm [20]. The wet ZnO film was subsequently dried in an oven at 100 °C overnight. Based on our previous work [30,31], the ZnO film was annealed at 500 °C for 2 h to achieve optimal crystalline structure. Subsequently, dispersed AuNPs (5 nm) were cast onto the surface of the ZnO film to form the ZnO/AuNPs heterostructure film. The final film was dried overnight at 100 °C.

2.2. Film characterizations

All measurements were performed at ambient conditions. Elemental, structural, and morphological characterizations were studied using XRF (NEX QC + Quanta EZ, R), XRD instrument (Malvern Panalytical Ltd), and SEM (FEI Quanta FEG 450). Additionally, optical absorption coefficient spectra were calculated using the following equation $\alpha = (1/d)\ln((1-R)/T)$, where T and R are the transmittance and reflectance spectra measured by UV–Vis spectrophotometer (U–3900H), and d is the film thickness. The bandgap energy was calculated using a Tauc plot according to the equation $(\alpha h\nu)^2 = \beta(h\nu - E_g)$ for direct bandgap semiconductors [29]. Additionally, 2D electrical conductivity maps were obtained using a Keithley 2450 source meter connected with a 4-point probe station (Microworld Inc.). The electrical conductivity was measured in the dark, under blue light irradiation (470 nm, 5 W) and UV light (366 nm, 5 W).

3. Results

Plasmon-exciton interaction occurs when a noble metal nanostructure is connected to semiconducting oxide nanostructure. From the SEM images, the ZnO film exhibits a smooth surface with agglomerated crystals of ZnO dispersed on the film surface (Fig. 1a). In contrast, the ZnO/AuNPs heterostructure film exhibits a homogeneous distribution (Fig. 1b).

Fig. 1c illustrates the typical XRF scans of pure ZnO and ZnO/AuNPs heterostructure films. The pure ZnO film shows the existence of Zn elements. In contrast, the ZnO/AuNPs heterostructure film contains about 28 % of Au elements and 72 % of Zn elements, confirming the existence of AuNPs on the ZnO film. Structural analysis was conducted using XRD patterns to confirm the heterostructure of the ZnO/AuNPs film (Fig. 1d). The pure ZnO film displays diffraction angles at 31.86°, 34.50°, 36.36°, 47.66°, and 56.66° corresponding to the Miller indices (100), (002), (101), (102), and (110) respectively, of a polycrystalline hexagonal wurtzite structure of ZnO (JCPDS 36–1451). In contrast, ZnO/AuNPs heterostructure film exhibits two additional diffraction peaks along with those of ZnO diffraction peaks, specifically, Au (111) and Au (200) at 37.50° and 43.50°, respectively. These peaks indicate that that AuNPs are polycrystalline with *fcc* cubic structure (JCPDS 04–0784). The lattice constants of the hexagonal ZnO film and cubic AuNPs were calculated using the following equations:

$$a_{ZnO} = \frac{\lambda}{\sqrt{3}\sin\theta_{100}} \quad (1)$$

$$c_{ZnO} = \frac{\lambda}{\sin\theta_{002}} \quad (2)$$

$$a_{AuNPs} = \frac{\sqrt{3}\lambda}{2\sin\theta_{111}} \quad (3)$$

where: λ is the X-ray wavelength (0.154184 nm). The lattice constants of ZnO films are $a = 3.25$ Å and $c = 5.20$ Å, as reported in the literature [16,19]. Similarly, the lattice constants of the ZnO in the ZnO/AuNPs heterostructure film are consistent with those of the ZnO film, confirming the superior crystallinity of the ZnO/AuNPs heterostructure film [9]. Additionally, The lattice constant of AuNPs is $a = 4.13$ Å, as accepted in the literature [32].

The excitation of localized surface plasmon resonances (LSPRs) excitation in a metal nanoparticle is illustrated as a coupling between an electromagnetic field and the coherent oscillation of all conduction electrons (Fig. 2a). Fig. 2b presents the absorption coefficient spectra of

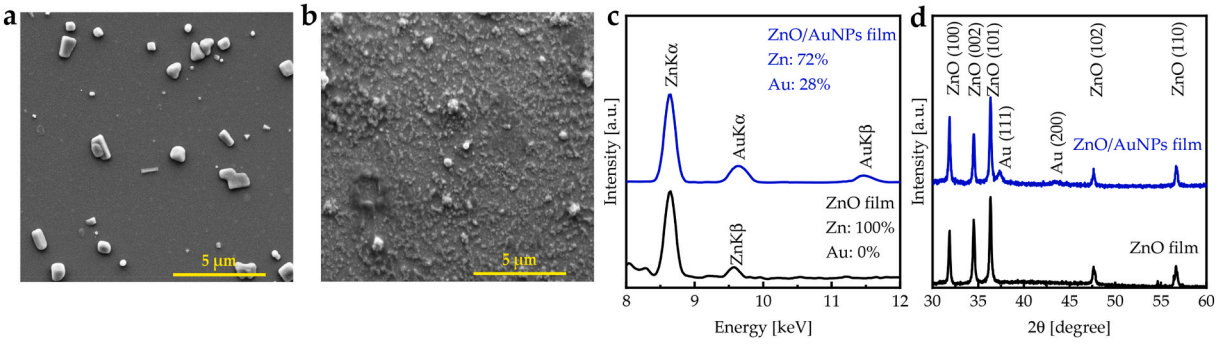

Fig. 1. SEM micrographs of **(a)** ZnO film and **(b)** ZnO/AuNPs heterostructure film. **(c)** XRF scans and **(d)** XRD patterns of ZnO film and ZnO/AuNPs heterostructure film.

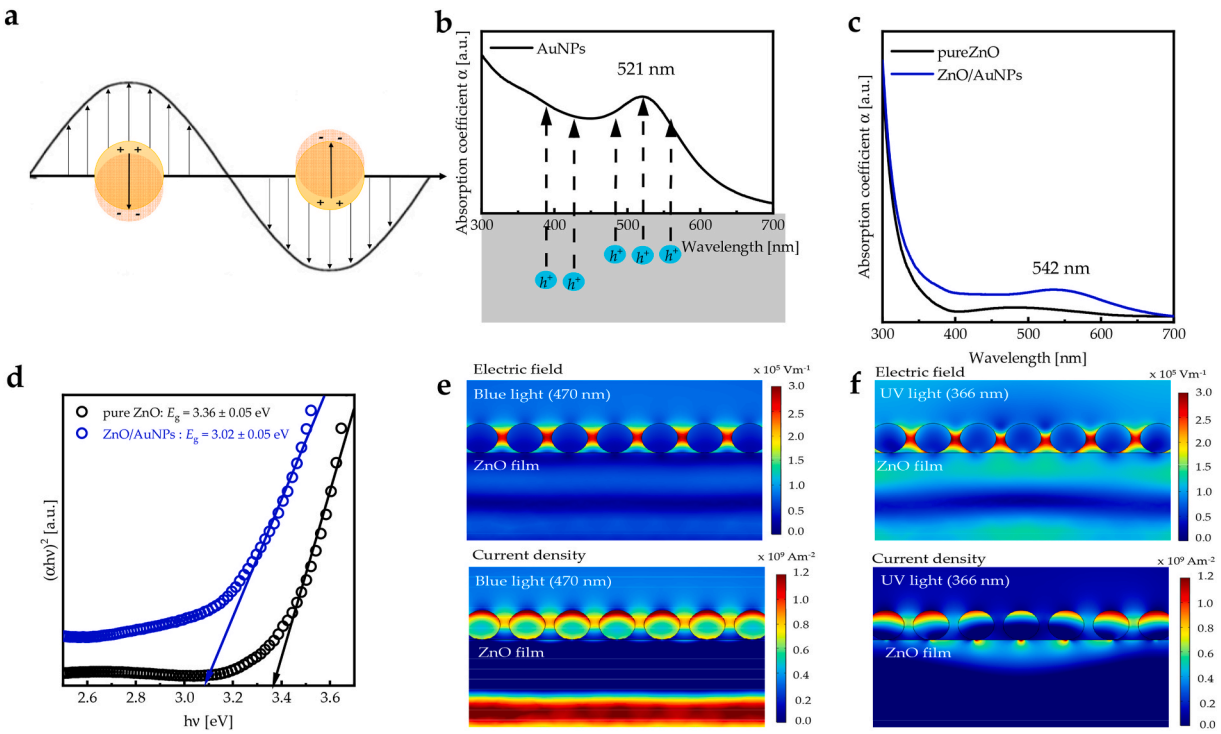

Fig. 2. Localized SPR excitation on spherical AuNPs: **(a)** EM-field-induced coherent localized oscillation of the electron cloud and **(b)** Absorption coefficient spectra of spherical AuNPs in the 300–700 nm spectral range with an illustration of hot carrier generation. **(c)** Absorption coefficient spectra of pure ZnO film and ZnO/AuNPs heterostructure film in the 300–700 nm spectral range. **(d)** Tauc plot of pure ZnO and ZnO/AuNPs films used to calculate the bandgap energy of both materials. COMSOL Multiphysics simulation of the electric field and electric density in ZnO/AuNPs heterostructure film: **(e)** under blue light irradiation (470 nm) and **(f)** under UV light irradiation (366 nm).

AuNPs in the spectral range of 300–700 nm. These spectra reveal an absorption band centered at 521 nm, indicative of the localized surface plasmon resonance of AuNPs. Upon LSPR excitation, the free electron oscillations generated energetic hot electrons and holes within a time range of 1–100 fs [33,34].

Fig. 2c illustrates the optical absorption coefficient spectra of the pure ZnO film and ZnO/AuNPs heterostructure film in the 300–700 nm spectral range. Both samples exhibit high absorption values in the UV region, with the ZnO/AuNPs heterostructure film showing a broad absorption band in the visible region. The UV band represents the absorption edge of the ZnO, whereas the visible band represents the LSPRs of the AuNPs within the ZnO/AuNPs heterostructure film. The plasmonic resonance band in the visible region exhibits redshifted and broadening compared to the spherical AuNPs (Fig. 2b), where the plasmonic resonance band of spherical AuNPs located at about 521 nm and the plasmonic resonance band of ZnO/AuNPs heterostructure film located at about 542 nm. This shift and broadening indicate strong interface damping of the plasmons through interacting with the excitons in ZnO. This implies the role of strong charge carrier interactions at the interface between Au and ZnO through the Schottky barrier [26]. Moreover, the plasmons of AuNPs affected the excitons in ZnO by shifting the absorption edge into the red region, which means decreasing the bandgap energy upon coating the ZnO layer with AuNPs (Fig. 2d). Specifically, the bandgap energy for ZnO film is approximately 3.36 ± 0.05 eV, consistent with literature values [16,35], while the ZnO/AuNPs heterostructure film exhibits a reduced bandgap energy of about 3.02 ± 0.05 eV. This reduction in bandgap energy is attributed to interactions between the excitons in ZnO and plasmons in Au through the Schottky barrier [26].

COMSOL Multiphysics simulations were conducted to study the electrical field and current density distribution in ZnO/AuNPs heterostructure film under UV and blue-light irradiation, aiming to understand the plasmon-exciton interactions. For these simulations, an we empolyed an electromagnetic wave interface and 2D geometry. The structure consisted of a ZnO film with a thickness of 500 nm and AuNPs with a thickness of 10 nm. Fig. 2e–f illustrate the electrical field and current density distribution in ZnO/AuNPs heterostructure film under UV and blue-light irradiation. Irradiated ZnO/AuNPs heterostructure film by blue light generated plasmon electrons between the AuNPs on the ZnO surface (Fig. 2e). The electric field is concentrated on the AuNPs due to the excitation of the plasmon electrons on the Au surfaces. Meanwhile, the current distribution is concentrated inside the ZnO films due to the interactions between the generated plasmonic electrons and the excitonic states in ZnO. Irradiating the ZnO/AuNPs heterostructure film with UV light generates the electron-hole pair within the ZnO film and interacts with the free electrons in AuNPs (Fig. 2f). Here, the electric field is concentrated on both the ZnO surface and the AuNPs, while, the current distribution is concentrated on the top of AuNPs and at the interface between the ZnO surface and AuNPs. This indicates that the generated electron-hole pairs within the ZnO film interact with the free electrons in AuNPs.

The electrical conductivity across the ZnO film exhibits low variation, with an average conductivity of 0.09 S cm^{-1} (Fig. 3a). This variation may stem from in the deposition process and film morphology. In contrast, the electrical conductivity increases from 0.09 to 3.56 S cm^{-1} upon coating the ZnO layer with AuNPs (Fig. 3b), which can be attributed to that the AuNPs play as contact regions on the ZnO surface. Electronic transport between AuNPs on the ZnO surface can occur via direct contact transport and electron tunneling betwee closely spaced AuNPs.

Now, to understand the effect of plasmons of AuNPs on the excitons of ZnO in the ZnO/AuNPs heterostructure film, the film was irradiated by blue light (λ = 470 nm). The electrical conductivity across the ZnO/AuNPs heterostructure film under blue light irradiation exhibits a steep increase up to 24.43 S cm^{-1} (Fig. 3c). This increase can be attributed to the plasmon-exciton interactions, which suppress the excitonic states in

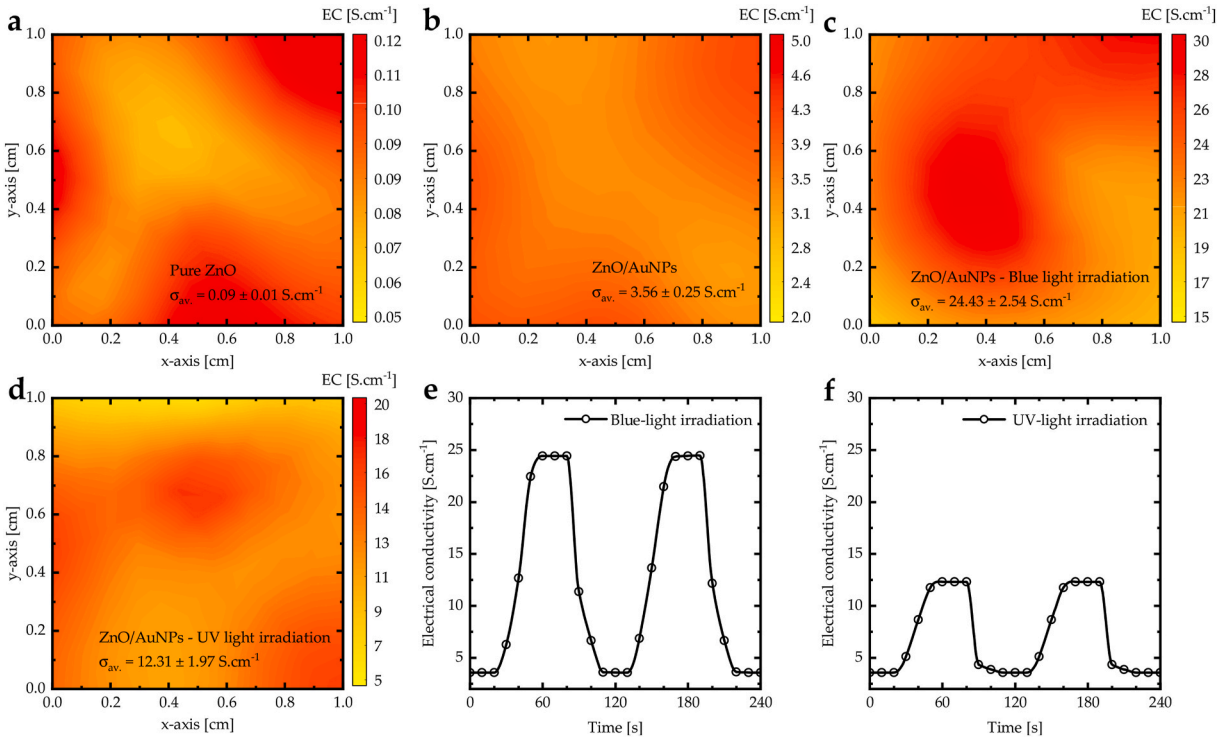

Fig. 3. 2D electrical conductivity maps of **(a)** pure ZnO film and **(b)** ZnO/AuNPs heterostructure film, **(c)** ZnO/AuNPs heterostructure film under blue light irradiation (470 nm), and **(d)** ZnO/AuNPs heterostructure film under UV light irradiation (366 nm) measured at 12 points through 1 cm × 1 cm on the film surface. Photoconductivity measurements of ZnO/AuNPs heterostructure film under **(e)** blue- and **(f)** UV light irradiation.

ZnO film and consequently enhance electron carrier mobility. Similarly, the electrical conductivity across the ZnO/AuNPs heterostructure film under UV light irradiation (λ = 366 nm) exhibits a steep increase up to 12.31 S cm^{-1} (Fig. 3d). This increase is attributed to the plasmon-exciton interactions, which promote electron conduction through the heterostructures.

Fig. 3e–f illustrates photoconductivity measurements of ZnO/AuNPs heterostructure film under blue- and UV-light irradiation as a function of time, respectively. The plasmon-exciton interactions enhance the photoconductivity with good consistency and repeatability. The photosensitivity of the ZnO/AuNPs photodetector can be evaluated using the following equation [36]:

$$Sens. = \left(\sigma_{ph} - \sigma_d\right) / \sigma_d \tag{4}$$

where σ_{ph} represents the photoconductivity and σ_d is the dark conductivity. The photosensitivity for ZnO/AuNPs under blue and UV lights is 586.2 % and 245.8 %, respectively. Additionally, the photoresponsivity of the photodetector can be evaluated using reference [37]:

$$Resp. = \sigma_{ph} / P_0 \ [\mathrm{S.W^{-1}cm^{-1}}] \tag{5}$$

The photoresponsivity of ZnO/AuNPs under blue and UV lights is 1.63 and 0.82 $S.W^{-1}cm^{-1}$, respectively. The rise time (τ_r) is defined as the time for taken for the photocurrent to increase from 10 % to 90 % of its maximum value ($\tau_r = \tau_{90\%} - \tau_{10\%}$). The decay time ($\tau_d$) is the time required for the photocurrent to decrease from 90 % to 10 % of its maximum value ($\tau_d = \tau_{10\%} - \tau_{90\%}$) [38,39]. The rise times of ZnO/AuNPs under blue and UV lights are 25 s and 23 s, respectively. Conversely, the decay times of ZnO/AuNPs under blue and UV lights are 20 s and 8 s, respectively.

4. Discussion

The plasmon-exciton interactions within the ZnO/AuNPs heterostructure film are explained by the energy band diagram (Fig. 4). In the ZnO film, there are no electronic interactions between ZnO and the surrounding media (glass and air) (Fig. 4a), leading to no changes in the excitonic state in ZnO (E_g = 3.36 eV). This is because there are no additional free electrons are from the surrounding media to disrupt the electron-hole pair (exciton) in the ZnO film. Conversely, upon blue- light irradiation, the oscillations of free electron on the Au surface generate plasmonic electrons and holes via electron transitions by photon absorption within a time range of 1–100 fs (Fig. 4b) [33,34].

When the electron-accepting orbital of ZnO is located near the Au surface, plasmonic electrons with sufficient energy can transfer from AuNPs into the conduction band in ZnO. This interaction between the plasmons in AuNPs and the excitons in ZnO is facilitated at energies of about 2.30 eV (localized surface plasmon resonance energy in ZnO/AuNPs heterostructure film) andabout 5.4 eV (The work function of gold). As a result, this leads to the suppression of the excitonic states in ZnO film (E_g = 3.02 eV).

Irradiated the ZnO/AuNPs heterostructure film by blue light (λ = 470 nm) generates the plasmonic electrons, which transfer to a ZnO film support via a plasmon-mediated electron-transfer (PMET) pathway [40–42]. Within the ZnO/AuNPs heterostructure film, the SPR excitation amplifies the generation of plasmonic electrons with high potential energy on the Au surface, facilitating their rapid and efficient transfer to the ZnO film. This transfer increases the electrical conductivity from 3.56 to 24.43 S cm^{-1} (Fig. 4c). The presence of Schottky barrier at ZnO/AuNPs interface helps trap the transferred plasmonic electrons in the conduction band of ZnO by delaying their return to the AuNPs [43].

Two pathways exist for interfacial electron transfer [44,45]. The indirect transfer of plasmonic electrons from the Au surface to ZnO involves a two-step pathway (Fig. 4d) [46,47]; first, plasmonic electron–hole pairs are generated in the AuNPs; second, these electrons transfer into the conduction band of the ZnO. Alternatively, direct transfer of plasmonic electrons can occur through the dephasing channel between the Au surface and electron-accepting orbitals of the ZnO (Fig. 4d) [45,48]. Since no holes are generated in the valence band of

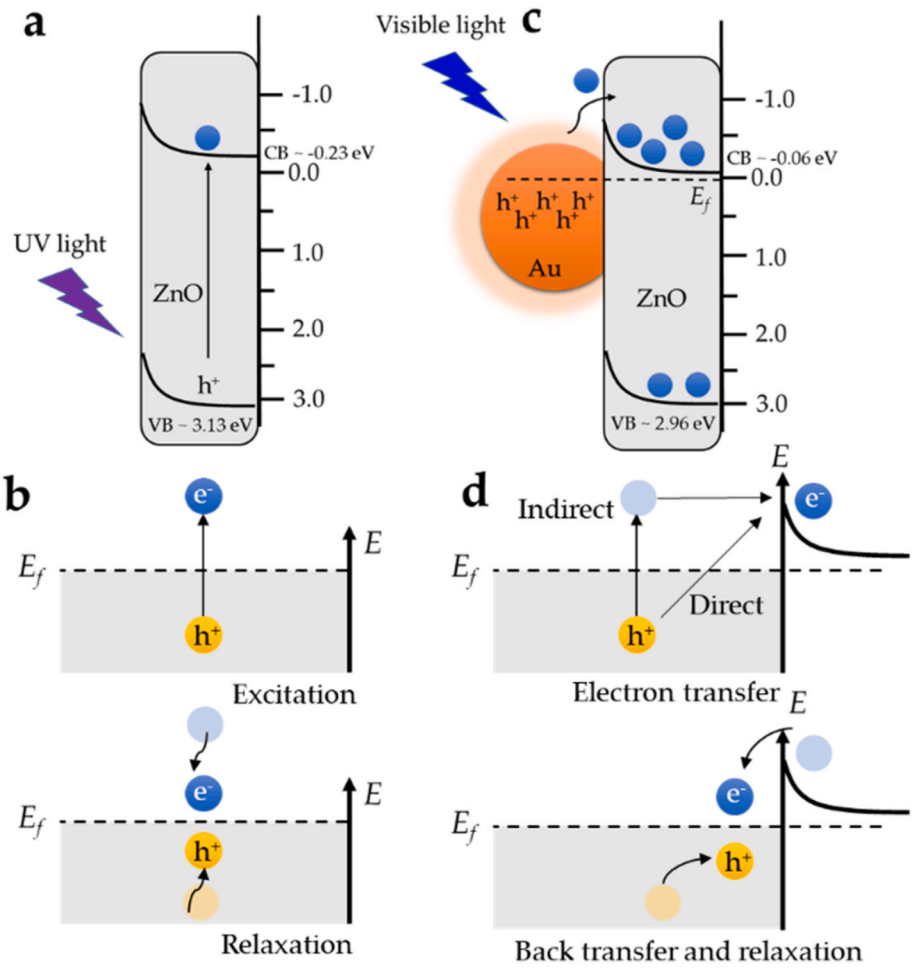

Fig. 4. Schematic model of plasmon-exciton interaction accompanied by corresponding energy band diagram for **(a)** ZnO film and **(b)** ZnO/AuNPs heterostructure film. **(c)** Plasmon-induced hot carrier generation and **(d)** hot electron transfer/back-transfer processes in metal and metal/semiconductor systems.

ZnO film under visible light, the plasmonic electrons transferred to ZnO film have a longer lifetime, allowing them to participate in chemical reactions in photocatalysts or produce photocurrents in photovoltaic devices [49,50]. These transferred plasmonic electrons diffuse into the defect states, trapping at various electronic states within the ZnO film, which have energy levels lower than that of the conduction band [51]. These recognized trapping states are known as oxygen vacancies, formed by removing oxygen atoms from the ZnO film [52].

Alternatively, irradiation of the ZnO/AuNPs film with UV light ($\lambda =$ 366 nm) generates the electron-hole pair within the ZnO film that interact with the free electrons in AuNPs, resulting in an increase in electrical conductivity from 3.65 to 12.31 S cm^{-1}. The effective plasmon-exciton coupling strength can be described by Hopfield Hamiltonian as follows [53],

$$H = H_0 + H_{int} \tag{7}$$

$$H = \left(\omega_{pl} a^{+} a + \omega_X b^{+} b\right) + \left(\Omega_R (a^{+} + a)(b^{+} + b) + \Omega_R^2 \,/\, \omega_X (a^{+} + a)^2\right) \tag{8}$$

where: H_0 represents the Hamiltonian of self-energies for the plasmon and exciton, H_{int} denotes the plasmon-exciton interaction terms, ω_{pl} is the plasmon frequency, ω_X is the single exciton frequency, Ω_R is the Rabi energy splitting, $a^{+}(a)$ and $b^{+}(b)$ are the plasmon and exciton creation (annihilation) operators. Based on the previous discussion, we can conclude that the effect of plasmons on the excitons is more significant than the effect of excitons on the plasmons. However, the plasmon-exciton interactions can enhance the photoconductivity with good consistency and repeatability.

5. Conclusions

In this study, we investigated the plasmon-exciton interactions between the AuNPs and ZnO within ZnO/AuNPs heterostructure film. The absorption coefficient spectra exhibit high values in the UV region for both ZnO and ZnO/AuNPs films. The broad band in the visible region for ZnO/AuNPs heterostructure film, representing the exciton band and localized surface plasmon resonances (LSPRs) of the AuNPs, respectively. The shifting of the plasmonic resonance band into the red region is attributed to the strong interface damping of the surface plasmons due to their interaction with excitons in ZnO. Moreover, the plasmons of AuNPs affected the excitons in ZnO leading to a shift in the absorption edge into the red region, indicating a decrease in the bandgap energy from 3.36 eV (for ZnO alone) to 3.02 eV (for ZnO/AuNPs). Irradiated the ZnO/AuNPs heterostructure film by blue light ($\lambda =$ 470 nm) generates the plasmonic electrons, and these electrons interact with the excitonic states in ZnO, which increases the electrical conductivity from 3.65 to 24.43 S cm^{-1}. On the other hand, irradiated the ZnO/AuNPs heterostructure film by UV light ($\lambda =$ 366 nm) generates the electron-hole pair within the ZnO film and interacts with the free electrons in AuNPs, which increases the electrical conductivity from 3.65 to 12.31 S cm^{-1}. The simulation conducted using COMSOL Multiphysics to analyze the charge density in ZnO/AuNPs heterostructure film under blue light irradiation (470 nm) and UV light irradiation (366 nm) successfully validated our findings. .

Declaration of competing interest

The authors declare that there is no conflict of interests or personal relationships that could have appeared to influence the work reported in this article.

Data availability

Data will be made available on request.

Acknowledgments

The scientific support by the Ministerium für Innovation, Wissenschaft und Forschung des Landes Nordrhein-Westfalen, the Senatsverwaltung für Wirtschaft, Technologie und Forschung des Landes Berlin, and the Bundesministerium für Bildung und Forschung is gratefully acknowledged.

References

[1] F. Davoodi, N. Talebi, Plasmon–exciton interactions in nanometer-thick gold-WSe2 multilayer structures: implications for photodetectors, sensors, and light-emitting devices, ACS Appl. Nano Mater. 4 (6) (2021) 6067–6074.
[2] A.H. Dorrah, N.A. Rubin, A. Zaidi, M. Tamagnone, F. Capasso, Metasurface optics for on-demand polarization transformations along the optical path, Nat. Photonics 15 (4) (2021) 287–296.
[3] F. Yoshihara, T. Fuse, S. Ashhab, K. Kakuyanagi, S. Saito, K. Semba, Superconducting qubit–oscillator circuit beyond the ultrastrong-coupling regime, Nat. Phys. 13 (1) (2017) 44–47.
[4] N.S. Mueller, et al., Deep strong light–matter coupling in plasmonic nanoparticle crystals, Nature 583 (7818) (2020) 780–784.
[5] T.K. Hakala, et al., Bose–Einstein condensation in a plasmonic lattice, Nat. Phys. 14 (7) (2018) 739–744.
[6] P. Vasa, C. Lienau, Strong light–matter interaction in quantum emitter/metal hybrid nanostructures, Acs Photonics 5 (1) (2018) 2–23.
[7] Y. Zhang, et al., Surface-plasmon-driven hot electron photochemistry, Chem. Rev. 118 (6) (2017) 2927–2954.
[8] P. Zhang, T. Wang, J. Gong, Mechanistic understanding of the plasmonic enhancement for solar water splitting, Adv. Mater. 27 (36) (2015) 5328–5342.
[9] P.-W. Shao, et al., Bicontinuous oxide heteroepitaxy with enhanced photoconductivity, Nat. Commun. 14 (1) (2023) 21.
[10] E. Muchuweni, T. Sathiaraj, H. Nyakotyo, Synthesis and characterization of zinc oxide thin films for optoelectronic applications, Heliyon 3 (4) (2017) e00285.
[11] G. Malik, S. Mourya, J. Jaiswal, R. Chandra, Effect of annealing parameters on optoelectronic properties of highly ordered ZnO thin films, Mater. Sci. Semicond. Process. 100 (2019) 200–213.
[12] J. Hu, J. Chen, T. Ma, Z. Li, Research advances in ZnO nanomaterials-based UV photodetectors: a Review, Nanotechnology 34 (23) (2023) 232002.
[13] K. Sandeep, S. Bhat, S. Dharmaprakash, Structural, optical, and LED characteristics of ZnO and Al doped ZnO thin films, J. Phys. Chem. Solid. 104 (2017) 36–44.
[14] S.K. Kokate, C.V. Jagtap, P.K. Baviskar, S.R. Jadkar, H.M. Pathan, K.C. Mohite, CdS sensitized cadmium doped ZnO solar cell: fabrication and characterizations, Optik 157 (2018) 628–634.
[15] S. Qiao, et al., ZnO nanowire based CIGS solar cell and its efficiency enhancement by the piezo-phototronic effect, Nano Energy 49 (2018) 508–514.
[16] I. Dhahri, et al., Optical and structural properties of ZnO NPs and ZnO–Bi2O3 nanocomposites, Ceram. Int. 48 (1) (2022) 266–277.
[17] L. Zhu, W. Zeng, Room-temperature gas sensing of ZnO-based gas sensor: a review, Sensor Actuator Phys. 267 (2017) 242–261.
[18] Q.M.A.-B. Mr, T.O.S. Mr, K.A. A.-i. Miss, Optical properties of hydrophobic ZnO nano-structure based on antireflective coatings of ZnO/TiO2/SiO2 thin films, Phys. B Condens. Matter 593 (2020) 412263.
[19] Q.M. Al-Bataineh, A. Alsaad, A. Ahmad, A. Al-Sawalmih, Structural, electronic and optical characterization of ZnO thin film-seeded platforms for ZnO nanostructures: sol–gel method versus ab initio calculations, J. Electron. Mater. 48 (2019) 5028–5038.
[20] A. Ahmad, A. Alsaad, Q. Al-Bataineh, M. Al-Naafa, Optical and structural investigations of dip-synthesized boron-doped ZnO-seeded platforms for ZnO nanostructures, Appl. Phys. A 124 (2018) 1–13.
[21] A. Alsaad, A. Ahmad, I. Qattan, Q.M. Al-Bataineh, Z. Albataineh, Structural, optoelectrical, linear, and nonlinear optical characterizations of dip-synthesized undoped ZnO and group III elements (B, Al, Ga, and In)-doped ZnO thin films, Crystals 10 (4) (2020) 252.
[22] A. Ahmad, A. Alsaad, Q. Al-Bataineh, Optical and Structural Characterization of Dip Synthesized Al-B Co-doped ZnO Seeded Platforms for ZnO Nanostructures, 2017.
[23] Q.M. Al-Bataineh, et al., Synthesis, crystallography, microstructure, crystal defects, optical and optoelectronic properties of ZnO: CeO2 mixed oxide thin films, Photonics 7 (4) (2020) 112. MDPI.
[24] G.A. Shi, M. Saboktakin, M. Stavola, S. Pearton, "Hidden hydrogen" in as-grown ZnO, Appl. Phys. Lett. 85 (23) (2004) 5601–5603.
[25] Y. Darma, et al., Plasmon–exciton interaction and screening of exciton in ZnO-based thin film on bulk Pt as analyzed by spectroscopic ellipsometry, Jpn. J. Appl. Phys. 56 (1S) (2016), 01AD06.
[26] N. Gogurla, R.K. Chowdhury, S. Battacharya, P.K. Datta, S.K. Ray, Plasmon charge transfer dynamics in layered Au–ZnO nanocomposites, J. Appl. Phys. 127 (5) (2020) 053105.
[27] V. Amendola, R. Pilot, M. Frasconi, O.M. Maragò, M.A. Iatì, Surface plasmon resonance in gold nanoparticles: a review, J. Phys. Condens. Matter 29 (20) (2017) 203002.
[28] G. Bertoni, et al., Nanoscale mapping of plasmon and exciton in ZnO tetrapods coupled with Au nanoparticles, Sci. Rep. 6 (1) (2016) 1–8.
[29] A. Ahmad, A. Migdadi, A. Alsaad, Q.M. Al-Bataineh, A. Telfah, Optical, structural, and morphological characterizations of synthesized (Cd–Ni) co-doped ZnO thin films, Appl. Phys. A 127 (12) (2021) 1–12.
[30] A.A. Ahmad, Q.M. Al-Bataineh, I.A. Aljarrah, A.D. Telfah, Electrochemical degradation of methyl red in zinc hydroxide and zinc oxide thin films, physical and chemical activation, Mater. Chem. Phys. 280 (2022) 125793.
[31] Q.M. Al-Bataineh, A. Alsaad, A. Ahmad, A. Al-Sawalmih, Structural, electronic and optical characterization of ZnO thin film-seeded platforms for ZnO nanostructures: sol–gel method versus ab initio calculations, J. Electron. Mater. 48 (8) (2019) 5028–5038.
[32] S.A. Fereig, G.M. El-Zaafarany, M.G. Arafa, M.M. Abdel-Mottaleb, Boosting the anti-inflammatory effect of self-assembled hybrid lecithin–chitosan nanoparticles via hybridization with gold nanoparticles for the treatment of psoriasis: elemental mapping and in vivo modeling, Drug Deliv. 29 (1) (2022) 1726–1742.
[33] M.L. Brongersma, N.J. Halas, P. Nordlander, Plasmon-induced hot carrier science and technology, Nat. Nanotechnol. 10 (1) (2015) 25–34.
[34] J.B. Khurgin, How to deal with the loss in plasmonics and metamaterials, Nat. Nanotechnol. 10 (1) (2015) 2–6.
[35] A. Ahmad, A. Migdadi, A. Alsaad, Q.M. Al-Bataineh, A. Telfah, Optical, structural, and morphological characterizations of synthesized (Cd–Ni) co-doped ZnO thin films, Appl. Phys. A 127 (12) (2021) 922.
[36] S.-J. Young, Y.-H. Liu, J.-T. Chien, Improving field electron emission properties of ZnO nanosheets with Ag nanoparticles adsorbed by photochemical method, ACS Omega 3 (7) (2018) 8135–8140.
[37] L. Yingying, C. Chuanwei, D. Xiang, G. Junshan, Z. Haiqian, Facile fabrication of UV photodetectors based on ZnO nanorod networks across trenched electrodes, J. Semiconduct. 30 (6) (2009) 063004.
[38] S.H. Zyoud, N.M. Ahmed, A.S.Z. Lahewil, A.F. Omar, Micro spot ZnO nanotubes using laser assisted chemical bath deposition: a low-cost approach to UV photodetector fabrication, Sensor Actuator Phys. 338 (2022) 113485.
[39] Y. Li, W. Zheng, F. Huang, All-silicon photovoltaic detectors with deep ultraviolet selectivity, PhotoniX 1 (1) (2020) 1–11.
[40] S.F. Hung, et al., Iridium oxide-assisted Plasmon-induced hot carriers: improvement on kinetics and thermodynamics of hot carriers, Adv. Energy Mater. 6 (8) (2016) 1501339.
[41] K. Qian, et al., Surface plasmon-driven water reduction: gold nanoparticle size matters, J. Am. Chem. Soc. 136 (28) (2014) 9842–9845.
[42] C. Clavero, Plasmon-induced hot-electron generation at nanoparticle/metal-oxide interfaces for photovoltaic and photocatalytic devices, Nat. Photonics 8 (2) (2014) 95–103.
[43] A. Furube, L. Du, K. Hara, R. Katoh, M. Tachiya, Ultrafast plasmon-induced electron transfer from gold nanodots into TiO2 nanoparticles, J. Am. Chem. Soc. 129 (48) (2007) 14852–14853.
[44] K. Wu, J. Chen, J.R. McBride, T. Lian, Efficient hot-electron transfer by a plasmon-induced interfacial charge-transfer transition, Science 349 (6248) (2015) 632–635.
[45] C. Boerigter, R. Campana, M. Morabito, S. Linic, Evidence and implications of direct charge excitation as the dominant mechanism in plasmon-mediated photocatalysis, Nat. Commun. 7 (1) (2016) 10545.
[46] A.M. Brown, R. Sundararaman, P. Narang, W.A. Goddard III, H.A. Atwater, Nonradiative plasmon decay and hot carrier dynamics: effects of phonons, surfaces, and geometry, ACS Nano 10 (1) (2016) 957–966.
[47] Y.K. Lee, C.H. Jung, J. Park, H. Seo, G.A. Somorjai, J.Y. Park, Surface plasmon-driven hot electron flow probed with metal-semiconductor nanodiodes, Nano Lett. 11 (10) (2011) 4251–4255.
[48] C. Boerigter, U. Aslam, S. Linic, Mechanism of charge transfer from plasmonic nanostructures to chemically attached materials, ACS Nano 10 (6) (2016) 6108–6115.
[49] L. Amidani, et al., Probing long-lived plasmonic-generated charges in TiO2/Au by high-resolution X-ray absorption spectroscopy, Angew. Chem. Int. Ed. 54 (18) (2015) 5413–5416.
[50] C. Sönnichsen, et al., Drastic reduction of plasmon damping in gold nanorods, Phys. Rev. Lett. 88 (7) (2002) 077402.
[51] C. Di Valentin, G. Pacchioni, A. Selloni, Reduced and n-type doped TiO2: nature of Ti3+ species, J. Phys. Chem. C 113 (48) (2009) 20543–20552.
[52] T.L. Thompson, J.T. Yates, Surface science studies of the photoactivation of TiO2 new photochemical processes, Chem. Rev. 106 (10) (2006) 4428–4453.
[53] F. Todisco, et al., Ultrastrong plasmon–exciton coupling by dynamic molecular aggregation, Acs Photonics 5 (1) (2018) 143–150.